

光学学报

基于随机光纤激光器的多奇点涡旋光束

马小雅¹, 叶俊^{1,2,3}, 梁峻锐¹, 何俊鸿¹, 张扬¹, 许将明^{1*}, 周朴^{1**}, 姜宗福^{1,2,3}¹国防科技大学前沿交叉学科学院, 湖南长沙 410073;²国防科技大学南湖之光实验室, 湖南长沙 410073;³国防科技大学高能激光技术湖南省重点实验室, 湖南长沙 410073

摘要 部分相干结构光束具有抗湍流闪烁和抑制散斑等特性,在大气传输和成像等领域具有广泛的应用潜力。提出并展示了基于随机光纤激光器产生的部分相干多奇点涡旋光束。对不同拓扑荷数涡旋光束的相干叠加进行仿真研究,发现叠加过程可产生具有多个奇点的复杂相位分布。采用中心波长为 1081.3 nm 的随机光纤激光器作为照明光源,通过搭建空间干涉环路实现多奇点涡旋光束的产生。奇点数目可通过改变参与干涉的涡旋拓扑荷数来实现灵活调控。该工作有望为多粒子控制、涡旋光通信、光学计算和成像等领域提供重要参考。

关键词 激光器; 随机光纤激光器; 多奇点涡旋; 涡旋叠加; 奇点可控; 部分相干

中图分类号 O436

文献标志码 A

DOI: 10.3788/AOS232013

1 引言

携带轨道角动量(OAM)的涡旋光束以其独特的螺旋相位分布和无限正交特性在光学通信、微粒操纵、量子加密和超分辨成像等领域展现出卓越的科研和应用价值^[1-5]。在多功能性操作和多样化应用需求的背景下,如何拓展涡旋光束的调控自由度已成为当前亟待解决的科学问题^[6]。相比仅有一个相位奇点的传统涡旋光束,利用将两个或多个涡旋光束进行相干叠加而生成多奇点涡旋光束可实现对相位奇点的符号、数量、分布等方面的精确控制,进而显著丰富了相位自由度的调控手段。2016年,上海大学的Huang等^[7]基于特定编码的全息图实现了两个、三个和四个拉盖尔-高斯(LG)光束的相干叠加。2018年,清华大学的Wan等^[8]利用空间失配的两个厄米-高斯光束的相干叠加获得了局部奇点可调节的多奇点涡旋光束。2021年,电子科技大学的Zeng等^[9]对涡旋光束和椭圆高斯光束的同轴叠加态进行理论研究,并实现了相位奇点的精确调控。2023年,上海理工大学的Gu等^[10]在理论上实现了在不同时空域中具有多个相位奇点的时空涡旋光束,且其横向OAM灵活可控。复杂的光强和相位分布使得多奇点涡旋光束能够蕴含更为丰富的光学信息,有望满足不断增长的通信带宽要求。2014年,洛桑第斯大学的Anguita等^[11]将涡旋叠加产生的多奇点涡旋光束应用到光学无线通信链路中,数据传

输速率高达 100 Gbit/s。2020年,上海交通大学和华中科技大学^[12]合作实现多涡旋光束的腔内直接产生,并验证了其在信息传输方面的应用潜力。2022年,深圳大学的Feng等^[13]将分数阶涡旋叠加态应用到加密通信领域,通过卷积神经网络进行解密,误码率低至 0.008%。同年,北京理工大学的Fu等^[14]基于方位角调制生成了多达 64 个分量的高均匀性 OAM 梳,这为涡旋复用通信和大容量数据传输等领域提供了优异光源。2023年,西安理工大学的王明军等^[15]对涡旋叠加光束在水下通信的传输特性进行了系统研究,表明多奇点涡旋光束具有抗水下湍流的能力。同年,北京理工大学的Li等^[16]从理论和实验上验证了一种光子总角动量的分离和调控方法,该方法有望应用于光学信息加密和通信传输等领域。西北工业大学的樊鑫豪等^[17]基于超表面对涡旋叠加态进行纵向调控,显著提升了信道中的模态容量。此外,多奇点涡旋光束也被证明在粒子捕获^[18]、光学计算^[19]等领域具有广泛的应用前景。

照明光源的特性会传递给其产生的结构光束,因此激光光源的选择对于结构光场的应用至关重要。相比高相干性结构光束,部分相干结构光束已被证明具有抗湍流闪烁、抑制散斑等效果,在大气传输、成像等领域表现出明显的优势^[20-21]。随机光纤激光器(RFL)基于无源光纤中的瑞利散射提供随机分布式反馈,不具备传统光纤激光器的谐振腔结构,具有结构简单、无

收稿日期: 2023-12-29; 修回日期: 2024-01-29; 录用日期: 2024-01-30; 网络首发日期: 2024-02-20

基金项目: 国家自然科学基金(62305391)、博士后创新人才支持计划(BX20190063)

通信作者: *jmxu1988@163.com; **zhoupu203@163.com

稳定纵模、时域稳定性高和波长调谐灵活等优势^[22-29]。特别地,由于随机光纤激光器在无序介质中多重随机散射的内在反馈机制,其在相同输出带宽下的时间相干性低于谐振腔结构光纤激光器^[24]。此外,随机光纤激光经多模光纤传输后即可实现较低空间相干性的输出^[30],在成像方面展现出优越性能。电子科技大学的饶云江课题组近年来在随机光纤激光的多模高功率输出^[31-32]方面取得连续突破,并将其应用到无散斑成像^[33]、散斑相关成像^[34]、生物成像^[35-36]等多个领域,大幅提高了成像质量;四川大学的 Wu 等^[37]报道了随机光纤激光器在鬼成像中的优异性能;清华大学的 Wang 等^[38]利用随机光纤激光器、窄线宽光纤激光器等 5 种光纤光源进行多模光纤图像传输,结果表明随机光纤激光器具有最优成像效果。随机光纤激光器的部分相干性激发了研究人员对于将其应用到横向模式调控方面的兴趣。本课题组于 2015 年通过错位熔接方式实现 LP₁₁ 模式的随机光纤激光输出^[39],并于 2021 年采用腔外调制器件实现了拓扑荷数可在 -50~50 范围内任意调控的涡旋随机光纤激光器^[40]。此外,英国阿斯顿大学^[41]以及中国科学技术大学^[42-44]、上海大学^[45]和深圳大学^[46-48]等单位已通过模式选择器、长周期光纤光栅等模式转换器件在随机光纤激光器中实现混合模、高阶模和柱矢量光束等横向高阶模式的可控输出。目前,研究人员已经以随机光纤激光器作为光源,实现多种典型结构光束,然而,尚无基于随机光纤激光器产生多奇点涡旋光束的报道。将随机光纤激光器的部分相干性与奇点可控的结构光束相结合,有望拓展结构光场的多维调控能力,在多阱光镊、自由空间光通信和散斑相关成像等领域具有重要应用前景。鉴于此,本文提出并展示了一种基于随机光纤激光器产

生多奇点涡旋光束的方法。基于两个 LG 光束相干叠加的理论模型,以自行研制的随机分布式反馈光纤激光器作为照明光源,利用空间调控器件实现高斯光束到 LG 光束的转换,通过具有不同拓扑荷数的 LG 光束之间的相干叠加实现奇点数目可控的多奇点涡旋光束。

2 理论模型及仿真结果

LG 光束是一种典型的相位涡旋光束,为方便起见,本文考虑位于柱坐标系源平面处的零阶 LG 光束,即径向指数 $p=0$ 、柱坐标参数 $z=0$,其光场分布^[49]可以描述为

$$E(r, \theta) = \alpha(r)\beta(r, l)e^{-i\theta}, \quad (1)$$

式中: r, θ 为柱坐标参数; l 为拓扑荷数; $\alpha(r) = \sqrt{2/\pi} / w_0 e^{-r^2/w_0^2}$, $\beta(r, l) = \sqrt{1/(|l|)!} (r\sqrt{2}/w_0)^{|l|}$, w_0 为束腰半径。利用拓扑荷数分别为 l_1 和 l_2 的两束零阶 LG 光束进行共轴叠加,得到的叠加光束光场分布为

$$E_c(r, \theta) = \alpha(r)\beta(r, l_1)e^{-i l_1 \theta} + \alpha(r)\beta(r, l_2)e^{-i l_2 \theta}. \quad (2)$$

采用两个拓扑荷数绝对值相等、符号相反的零阶 LG 光束相叠加,仿真得到的振幅和相位分布如图 1 所示。不同于零阶 LG 光束的环形光强分布,叠加光束的光强呈现中心对称的花瓣图样,花瓣数为单个拓扑荷绝对值的两倍。仿真模拟了拓扑荷数绝对值从 1 到 5、10、20 的涡旋光束叠加态,振幅分布图上的花瓣数相应地从 2 个增加到 10 个、20 个和 40 个。从相位分布图上看,这种叠加态不具有螺旋相位波前的特征, LG 光束原有的相位奇点被湮灭,叠加光场为相位均匀的结构光场,仅在光强分布上呈现不同于 LG 光束的特殊分布。

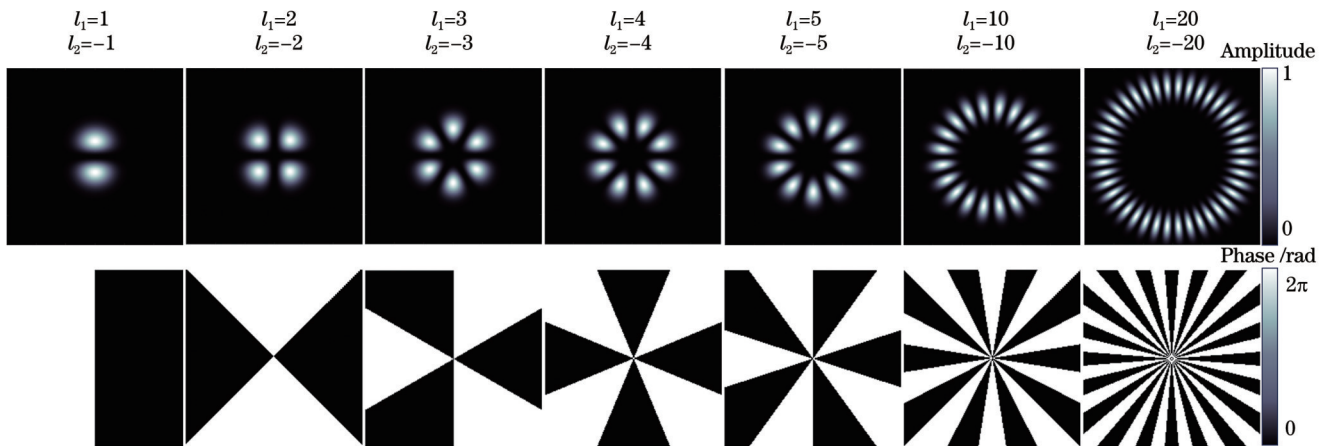


图 1 由拓扑荷数绝对值相等、符号相反的 LG 涡旋光束相叠加得到的振幅和相位分布

Fig. 1 Amplitude and phase distributions generated by LG vortex beam superpositions with equal absolute value and opposite sign of topological charges

图 2、图 3 和图 4 分别显示将拓扑荷数绝对值不等且符号相反、拓扑荷数绝对值不等且符号均为正,以

及拓扑荷数绝对值不等且符号均为负的零阶 LG 光束相叠加所得到的振幅和相位分布。这种叠加态保留

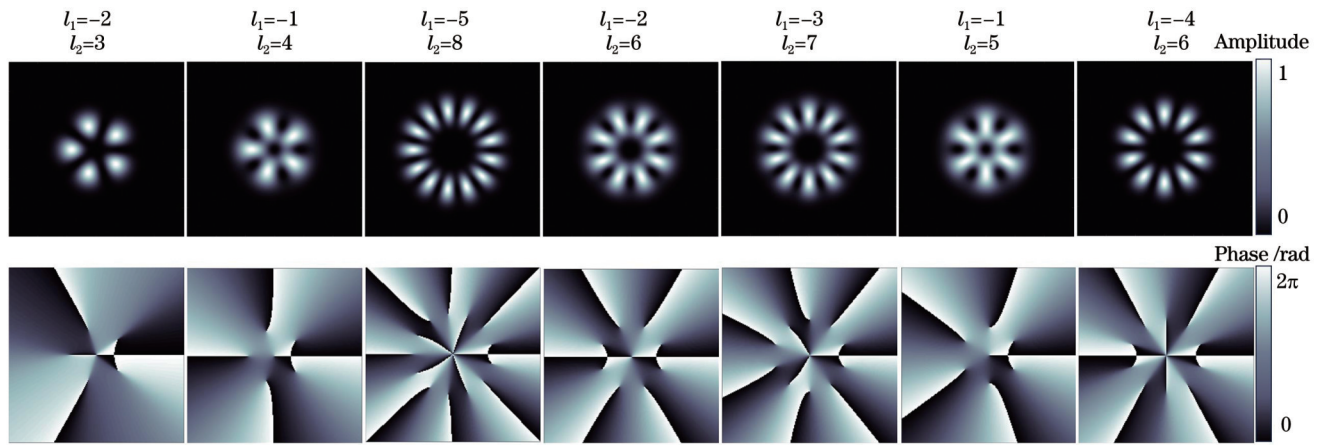


图 2 由拓扑荷数绝对值不等、符号相反的 LG 涡旋光束相叠加得到的振幅和相位分布

Fig. 2 Amplitude and phase distributions generated by LG vortex beam superpositions with unequal absolute value and opposite sign of topological charges

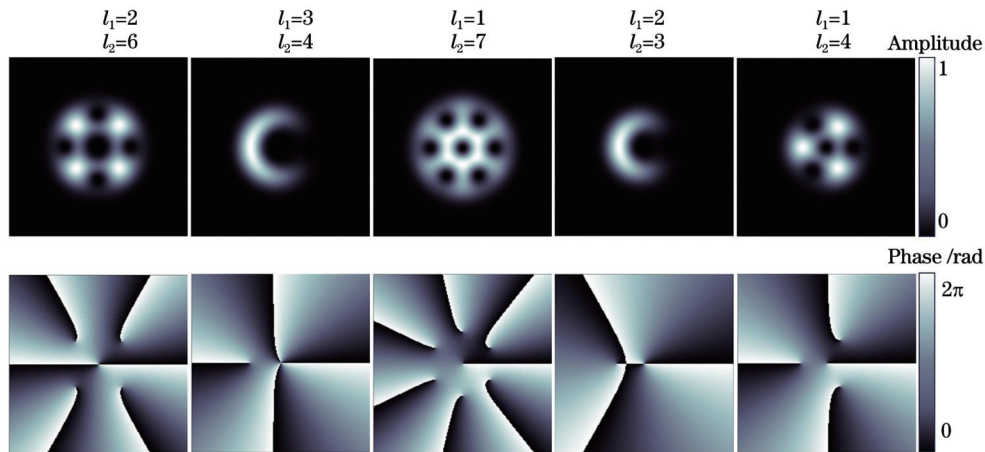


图 3 由拓扑荷数绝对值不等、符号为正的 LG 涡旋光束相叠加得到的振幅和相位分布

Fig. 3 Amplitude and phase distributions generated by LG vortex beam superpositions with unequal absolute value of positive topological charges

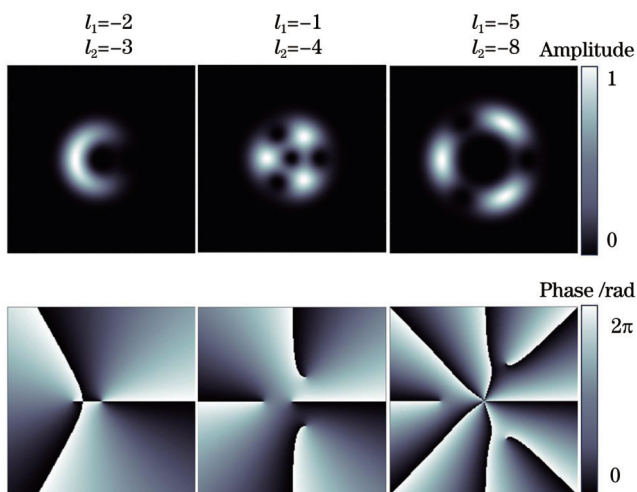


图 4 由拓扑荷数绝对值不等、符号为负的 LG 涡旋光束相叠加得到的振幅和相位分布

Fig. 4 Amplitude and phase distributions generated by LG vortex superpositions with unequal absolute value of negative topological charges

了螺旋相位分布的特性,并呈现出更为复杂的相位分布和丰富的光强分布图案。叠加光强仍然呈现中心对称的花瓣图样,花瓣数目为两个拓扑荷数相减的绝对值。花瓣数目相同的涡旋叠加态可能具有不同的光强分布,如拓扑荷数分别为-1和-4的涡旋叠加态与拓扑荷数分别为-5和-8的涡旋叠加态都具有三个花瓣,但两者的花瓣间距不同,后者的间距较大,这是由参与叠加的 LG 光束直径不同所导致的。相位分布图显示拓扑荷数绝对值较小的涡旋相位分布在中心位置,被拓扑荷数较大的涡旋相位包围。与 LG 光束的单个相位奇点不同,这种涡旋叠加除了产生位于中心位置的相位奇点外,还由于两个 LG 光束的相位耦合而产生新的相位奇点,新生奇点个数为 $|l_1 - l_2|$,总奇点个数为 $|l_1 - l_2| + 1$ 。中心奇点的拓扑荷数对应于两个 LG 光束中直径较小的涡旋拓扑荷数,新生奇点的拓扑荷数绝对值均为 1 且围绕中心奇点均匀分布。值得注意的是,图 3 和图 4 中新生奇点的拓扑荷数绝对值均为 1,但符号相反,这是由参与叠加的两个

LG 光束中直径较大光束的拓扑荷数的符号不同所致。

3 实验结构及结果讨论

3.1 实验结构

随机光纤激光器产生多奇点涡旋光束的实验结构如图 5 所示。随机光纤激光器采用后向泵浦的半开腔结构,如图 5(a)所示。泵浦光由自行搭建的激光二极管(LD)泵浦 1030 nm 掺镱光纤振荡器提供,对输出端进行泵浦倾泻(CPS)处理以滤除包层光。一个环形器(Cir)接在 1030 nm 光纤振荡器后用来保护泵浦源不受后向回光影响。随后,1030 nm 泵浦光通过 1030 nm/1080 nm 波分复用器(WDM)注入一段 5 km 的单模无源光纤(SMF,纤芯直径/包层直径为 8 μm /125 μm)中,产生的 1080 nm 信号光被高反光纤光栅(HR FBG,中心波长为 1081.3 nm,反射带宽为

0.07 nm,反射率 $>99\%$)反射,经由波分复用器后向输出。在随机光纤激光器中,激光增益由单模光纤的受激拉曼散射提供,激光反馈由单模光纤的随机分布式散射和高反光栅的点反馈共同提供。以该随机光纤激光器为照明光源,搭建如图 5(b)所示的空间光路实现多奇点结构光场的调控。由随机光纤激光器出射的高斯光束经准直扩束后,通过两个偏振分束器(PBS1、PBS2)和一个半波片(HWP)出射为偏振度较高且强度可调的水平线偏振光,经过 50:50 非偏振分束器(BS)分成透射和反射两路光束,反射后分别入射到空间光调制器(SLM)的不同位置。在空间光调制器上加载不同相位图,即可得到两束具有不同拓扑荷数的涡旋光束。这两束涡旋光经过反射后再次通过非偏振分束器进行干涉,形成具有复杂光强和相位分布的涡旋叠加态。叠加光束的光强通过透镜聚焦,由 CCD 相机收集。

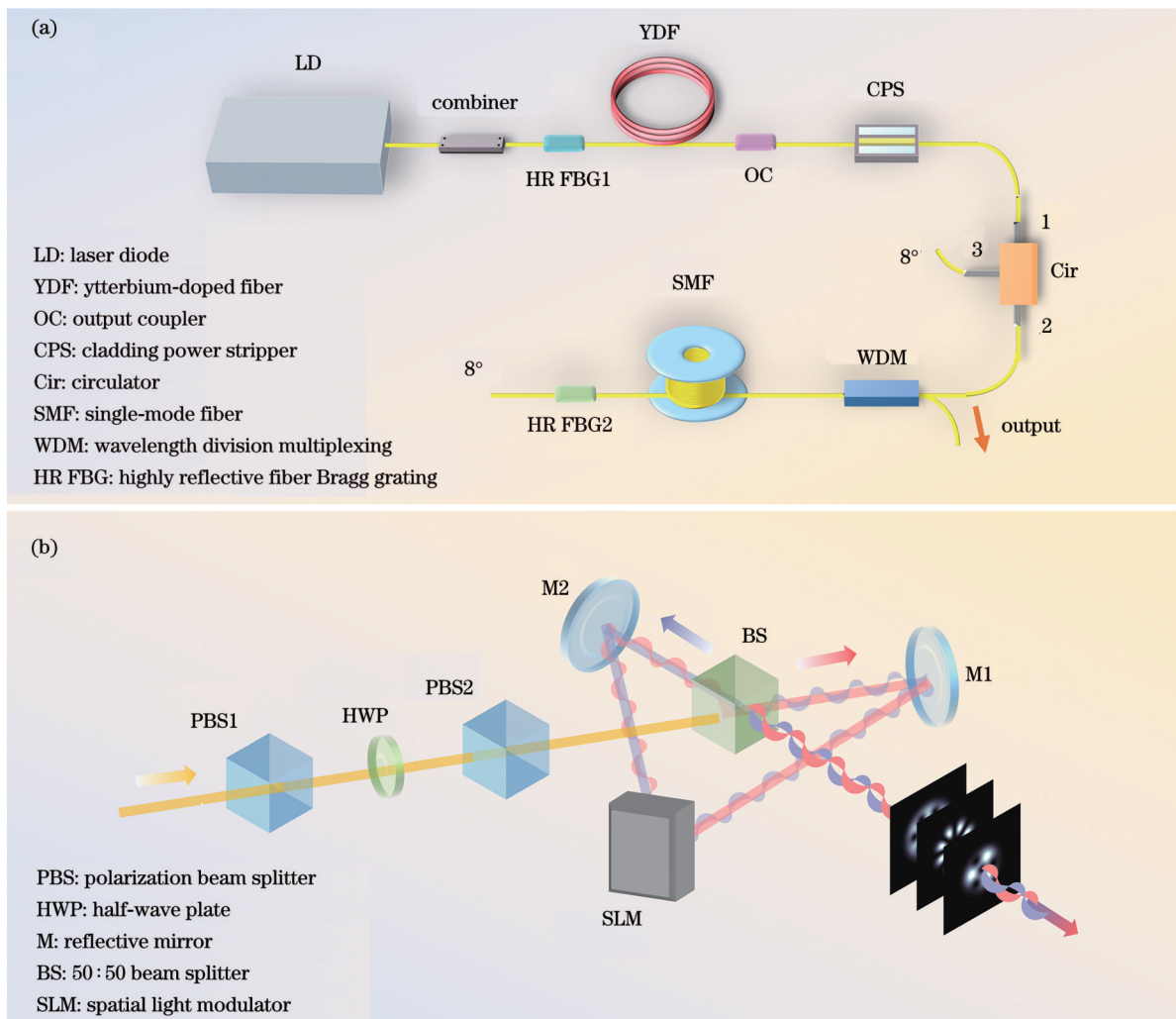


图 5 实验装置图。(a)随机光纤激光器实验结构图;(b)多奇点涡旋光束的产生光路图

Fig. 5 Experimental setups. (a) Structural diagram of RFL; (b) generation of spatial path of multi-singularity vortex beam

3.2 分析与讨论

随机光纤激光器的输出功率、对应的光谱和线宽等特性如图 6 所示。图 6(a)给出了随机光纤激光输出

功率随泵浦功率的演化曲线。随机激光在泵浦功率增加到 2.36 W 附近时产生,并随着泵浦功率的持续增加而近似呈线性增长,对应的斜率效率约为 58.91%。在

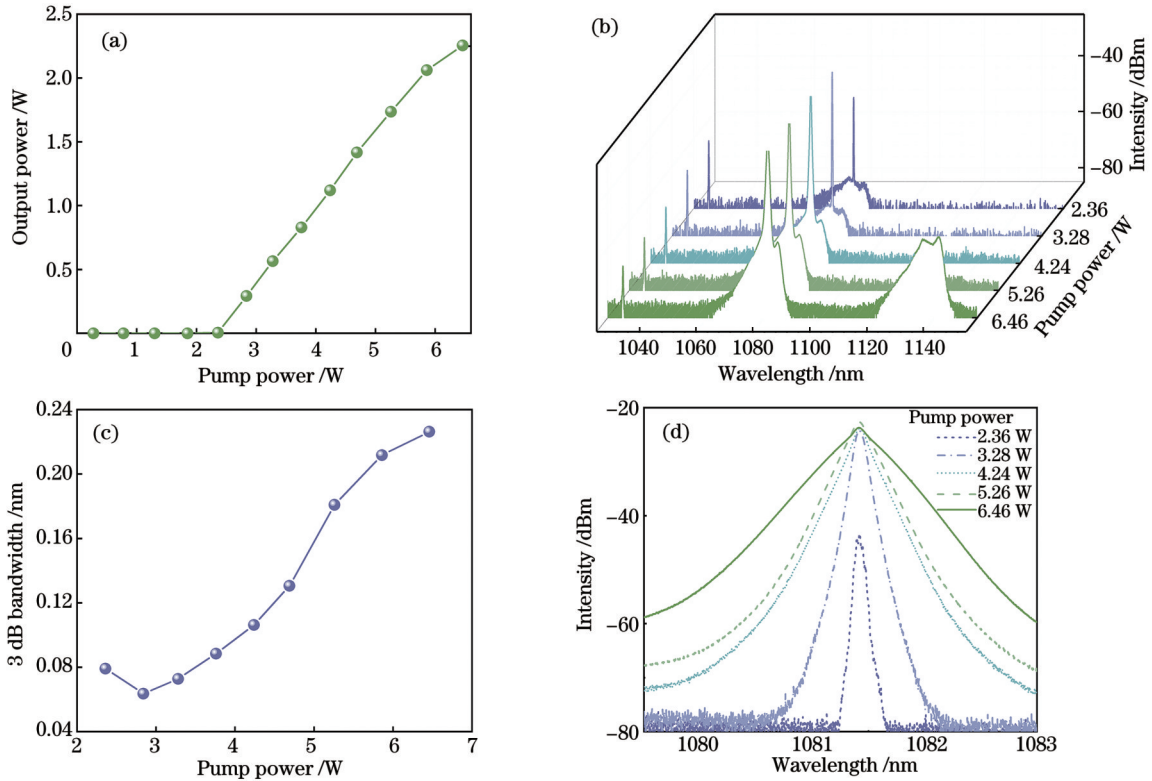


图6 随机光纤激光器的输出特性。(a)输出功率随泵浦功率的演化曲线;(b)不同泵浦功率下的输出光谱图,波长范围1025~1155 nm;(c)3 dB带宽随泵浦功率的演化曲线;(d)不同泵浦功率下信号光的输出光谱图,波长范围1079.5~1083 nm
 Fig. 6 Output characteristics of RFL. (a) Evolution of output power with pump power; (b) output spectra under different pump power, with wavelength range of 1025–1155 nm; (c) evolution of 3 dB bandwidth with pump power; (d) signal spectra under different pump power, with wavelength range of 1079.5–1083 nm

泵浦功率增加到5.46 W后,随机激光的输出功率增长率变缓,这是由受激拉曼散射效应产生新的波长成分所致。图6(b)表示不同泵浦功率下的输出光谱,测量范围为1025~1155 nm,光谱分辨率为0.1 nm。得益于随机光纤激光器的后向泵浦结构以及泵浦倾泻的处理,1030 nm泵浦光被充分转化为信号光或被倾泻,剩余泵浦成分较少。随着泵浦功率从2.36 W增加到5.26 W,随机激光的光谱占比逐渐增大,中心波长位于1081.3 nm。值得注意的是,在1070~1090 nm波长范围内,在信号光的较低强度处产生较宽的波长成分,这是由自发辐射放大效应所致。泵浦功率为3.28 W时,信噪比达到最大,为46.38 dB。在最大泵浦功率下,可以看到在1120~1150 nm的波长范围出现新的光谱成分,其光谱轮廓与无源硅基光纤的拉曼增益谱线十分相近,对应于受激拉曼散射效应产生的斯托克斯光。两个拉曼峰的波长位于1136 nm和1141 nm,是由1081.3 nm信号光分别通过 ≈ 13.6 THz和 ≈ 14.8 THz的拉曼频移产生。斯托克斯光功率增长迅速,这限制泵浦光的有效转化,抑制信号光功率的进一步增长。在最大泵浦功率下,随机激光的输出功率为2.26 W。此外,从图6(b)的光谱图上可看出随机激光的输出线宽随泵浦功率的增加而有所展宽,其

3 dB线宽的演化曲线如图6(c)所示。泵浦功率为2.84 W时,随机激光的3 dB线宽最小,为63.6 pm。随着泵浦功率的逐渐增加,3 dB线宽展宽,在最大泵浦功率下达到0.23 nm。泵浦功率为2.36 W对应的3 dB线宽较宽,为79.2 pm,这是由随机激光在产生阈值附近的输出不稳定所致。随机激光的精细光谱轮廓如图6(d)所示,测量范围为1079.5~1083 nm,光谱分辨率为0.02 nm,可以看到随机激光的光谱强度和输出线宽均随泵浦功率的增加而逐渐增大。尽管所用的高反光栅具有较窄的反射带宽,但由于1030 nm光纤振荡器的时域相对不稳定,强时域起伏会传递给产生的随机激光,这进一步增强自相位调制效应,导致随机激光的3 dB线宽展宽。同时,自相位调制可实现相位匹配的四波混频,产生新的频率成分。在这两种非线性效应的共同影响下,随机激光的光谱显著展宽,出现明显的拖尾^[50]。如需抑制光谱展宽,可采用时域较为稳定的泵浦源(如超荧光光纤激光器),这有助于抑制非线性效应,获得更窄的光谱线宽^[51]。

为了实现具有不同拓扑荷数的两个涡旋的相干叠加,需要在空间光调制器上加载两个全息光栅图,通过调整三角光路使由非偏振分束器出射的透射光束和反射光束分别打在空间光调制器上两个全息光栅图的中

心位置。涡旋光束经过奇数次反射时,其拓扑荷数的符号改变;经过偶数次反射时,其拓扑荷数的符号不变^[49]。受实验平台大小的限制,叠加光束经非偏振分束器出射后先经由一个反射镜反射到空旷处,再到达聚焦透镜。在图 5(b)的干涉光路中,由非偏振分束器出射的透射光束经空间光调制器转换成涡旋光束之后,在到达 CCD 之前共经过两次反射,而反射光束加载上涡旋相位后共经过三次反射到达 CCD,也就是说,前者的拓扑荷数符号不变,而后的拓扑荷数符号变为反向。因此,反射光束所加载的闪耀光栅应为反方向。实验中设置透射光束的拓扑荷数为 l_1 ,反射光束的拓扑荷数为 l_2 ,所设置的全息光栅图和对应该得到的 LG 涡旋叠加态如图 7~10 所示。全息光栅图为两个并列的闪耀光栅,左侧光栅对应透射光束的拓扑荷数 l_1 ,右侧光栅对应反射光束的拓扑荷数 l_2 。闪耀光栅

中心的叉形开口向下,所加载的拓扑荷数为正值,反之则为负值。图 7 给出了拓扑荷数绝对值相等、符号相反的涡旋叠加光斑与对应的全息光栅图,可以看到右侧光栅所加载的拓扑荷数为 $-l_2$,而其所得到的涡旋光束拓扑荷数为 l_2 ,这是由于反射光束经过奇数次反射到达 CCD 时拓扑荷数符号变为反向所致。例如,加载拓扑荷数 $l_1=5$ 与 $l_2=5$ 的全息光栅图得到的是 $l_1=5$ 与 $l_2=-5$ 的涡旋叠加态。叠加光强呈清晰可辨的花瓣图样,与图 1 所示的仿真结果十分相近。随着拓扑荷数绝对值的增加,叠加光束的直径逐渐增大。实验中所用的聚焦透镜焦距较长($f=750$ mm)导致拓扑荷数绝对值较大的涡旋叠加态(如 $|l_1|=|l_2|=10,20$)的束腰半径较大,通过更换焦距短一些的聚焦透镜可优化光斑形态。每个涡旋叠加态的花瓣数为单个拓扑荷绝对值的两倍,这与仿真结果一致。

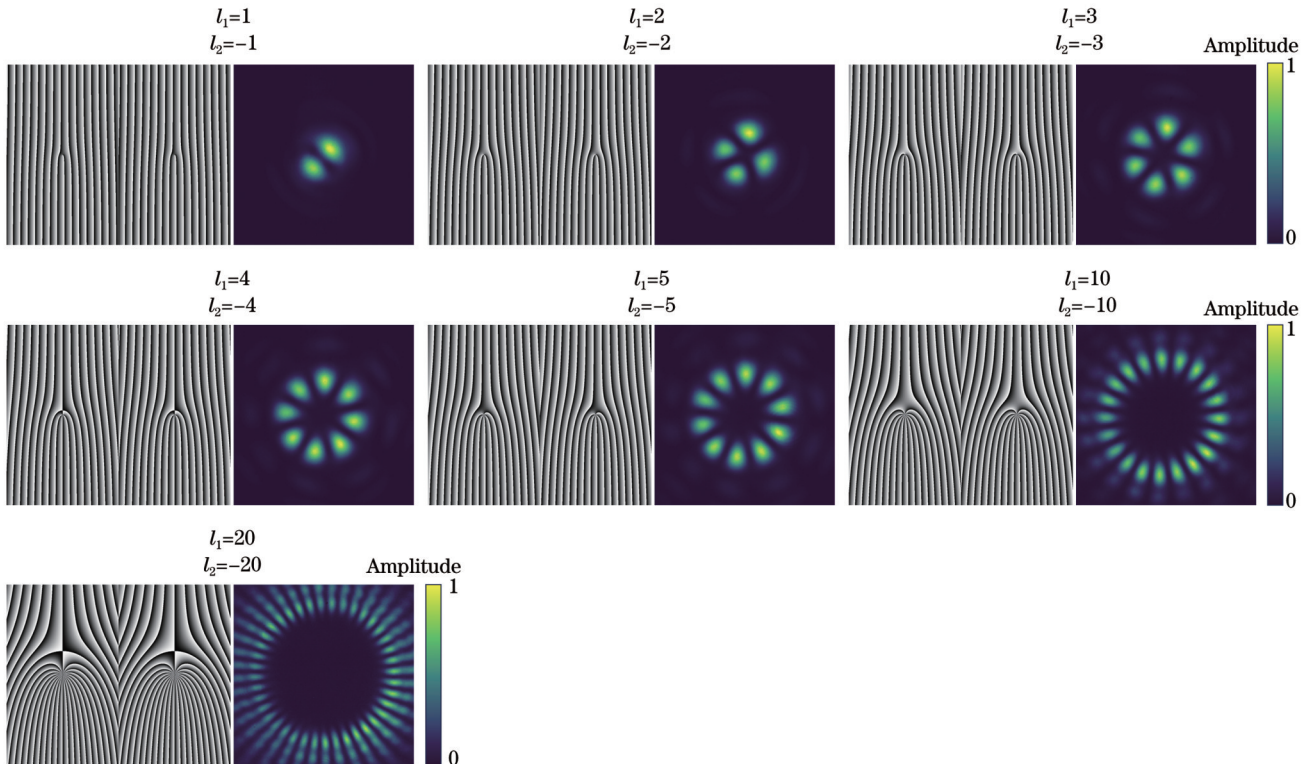


图 7 拓扑荷数绝对值相等、符号相反的 LG 涡旋光束叠加态与对应的全息光栅图

Fig. 7 LG vortex beam superpositions with equal absolute value and opposite sign of topological charges, and corresponding holographic gratings

由于空间光调制器的固有转换效率、非偏振分束器的分束光强不完全相等、两路干涉光束的光轴无法绝对重合等多重因素的影响,叠加光场中除了涡旋叠加光束之外,还存在少量残留的传统涡旋光束和未转化的高斯光束,这导致叠加光斑的花瓣附近和光斑中心的光强不为零、花瓣图案与背景的对比度降低、花瓣形状轻微变形等现象。为评估叠加光束的模式纯度,采用成像质量评价体系中的结构相似性(SSIM)指数^[52]。结构相似性指数可从亮度、对比度和相似度三

个方面综合评价重建图像和原始图像的相似性,取值范围为 0 到 1,其值越大表示重建图像质量越高。利用实验得到的叠加光强(图 7)与仿真叠加光强(图 1)进行计算,得出的结构相似性指数越大,表示叠加光束的光强对比度越高,实验结果与仿真结果越相近,即模式纯度越高。对于图 7 中拓扑荷数绝对值为 1~5 的涡旋叠加态,其结构相似性指数分别为 0.757、0.735、0.697、0.491、0.551。然而,空间光调制器的液晶排列引起的衍射效应导致叠加光斑外围出现残影,

且随着光斑尺寸的增大残影愈加明显,致使光强对比度下降、模式纯度评估误差增大。在这种情况下,应以受器件等不可抗力因素影响最小的评估数据为标准,实验所得叠加光束的结构相似性指数大于 0.7,具有较高模式纯度。

图 8 为拓扑荷数绝对值不等、符号相反的涡旋叠加态与对应的全息光栅图,右侧光栅所加载的拓扑荷数为 $-l_2$,花瓣数为两个拓扑荷数相减的绝对值。例如:加载 $l_1=-5$ 与 $l_2=-8$ 的全息光栅图得到的是 $l_1=-5$ 与 $l_2=8$ 的涡旋叠加态,花瓣数为 $|-5-8|=13$ 个;加载 $l_1=-3$ 与 $l_2=-7$ 的全息光栅图得到的是 $l_1=-3$ 与 $l_2=7$ 的涡旋叠加态,花瓣数为 $|-3-7|=10$ 个。这种涡旋叠加态的光斑中间存在一个相位奇点,其拓扑荷数为参与叠加的两束 LG 光束之间较小的拓扑荷数,除此之外还在两束 LG 光束的相位耦合处产生新的相位奇点,其拓扑荷数绝对值为 1,数目为两个拓扑荷数相减的绝对值且围绕中心均匀分布。以 $l_1=-3$ 、 $l_2=7$ 和 $l_1=-4$ 、 $l_2=6$ 的两种涡旋叠加光束为例,两者

的花瓣数目和新生奇点数目均为 10,但可观察到中心奇点的大小和光斑大小各不相同:前者的中心奇点较小、光斑直径较大;而後者的中心奇点较大、光斑直径较小。这是因为中心奇点的大小由拓扑荷数较小的 LG 光束决定,光斑直径则由拓扑荷数较大的 LG 光束决定。同理, $l_1=-2$ 、 $l_2=3$ 和 $l_1=-1$ 、 $l_2=4$ 的两种涡旋叠加光束也具有相似的特征。图 9 和图 10 分别表示实验所得到的绝对值不等的正拓扑荷数和负拓扑荷数的涡旋叠加态及其所对应的全息光栅图。这种叠加也保留了螺旋相位分布并生成更为复杂的奇点光场,叠加光强呈现丰富的瓣状图样。其中 $l_1=3$ 与 $l_2=4$ 、 $l_1=2$ 与 $l_2=3$ 、 $l_1=-2$ 与 $l_2=-3$ 三种涡旋叠加光束仅产生一个新的相位奇点,位于中心一侧。此外,拓扑荷数分别为 1 和 4 的涡旋叠加态与拓扑荷数分别为 -1 和 -4 的涡旋叠加态具有相同的光强分布和奇点数目,但围绕中心分布的新生奇点的拓扑荷数不同:前者为 1,符号对应于拓扑荷数为 4 的 LG 光束;后者为 -1,符号对应于拓扑荷数为 -4 的 LG 光束。

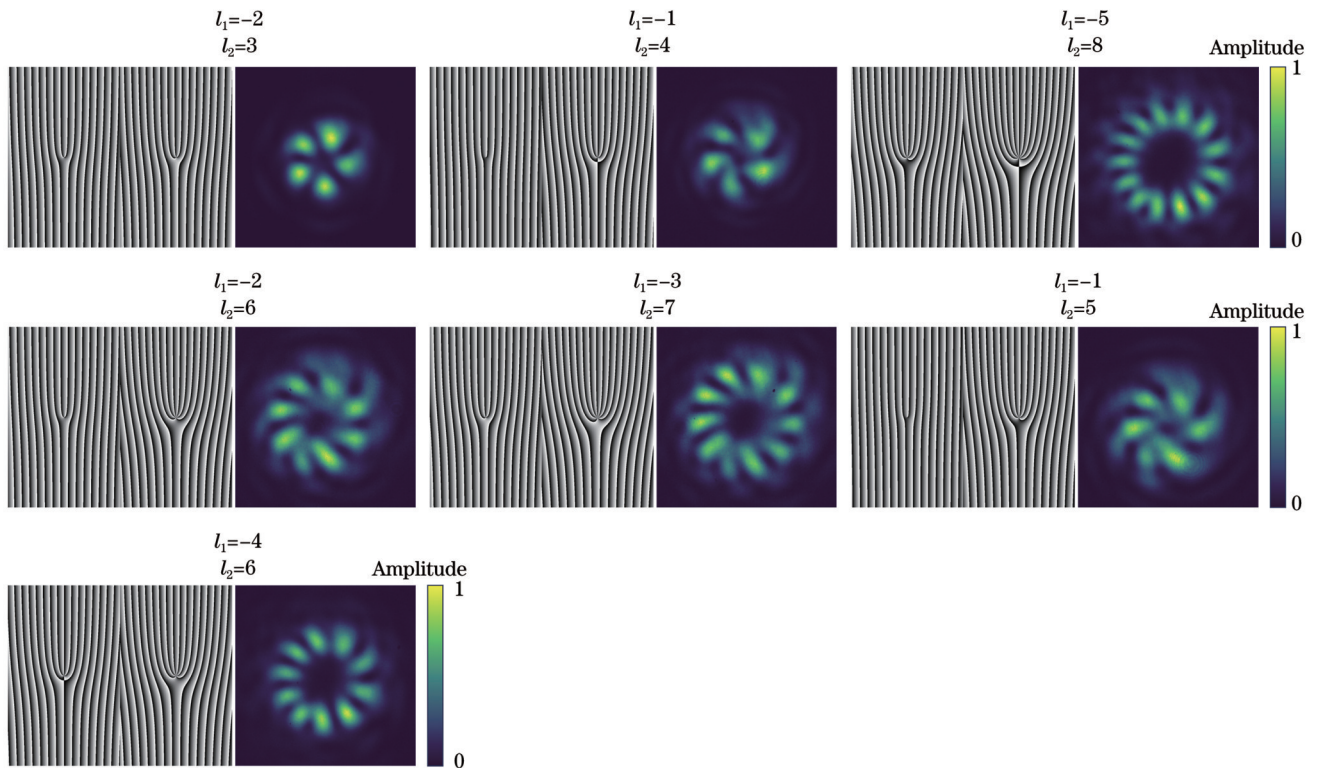


图 8 拓扑荷数绝对值不等、符号相反的 LG 涡旋光束叠加态与对应的全息光栅图

Fig. 8 LG vortex beam superpositions with unequal absolute value and opposite sign of topological charges, and corresponding holographic gratings

根据以上讨论,两路涡旋光束的相干叠加即为两种不同轨道角动量的相干叠加。拓扑荷数绝对值相同、符号不同的两种涡旋光束具有方向相反的等值轨道角动量,在叠加过程中轨道角动量相互湮灭,产生不具有螺旋相位分布的花瓣状叠加光束;拓扑荷数绝对值不同的两种涡旋光束具有不相等的轨道角动量,在

叠加过程中轨道角动量相互耦合,产生具有更多相位奇点的涡旋光束。利用图 5(b)中的三角干涉光路,通过改变空间光调制器上加载的全息光栅图,可实现不同螺旋相位分布的涡旋相干叠加,产生具有不同相位奇点分布的叠加光场,从而实现多奇点涡旋光束的产生与奇点数目调控。

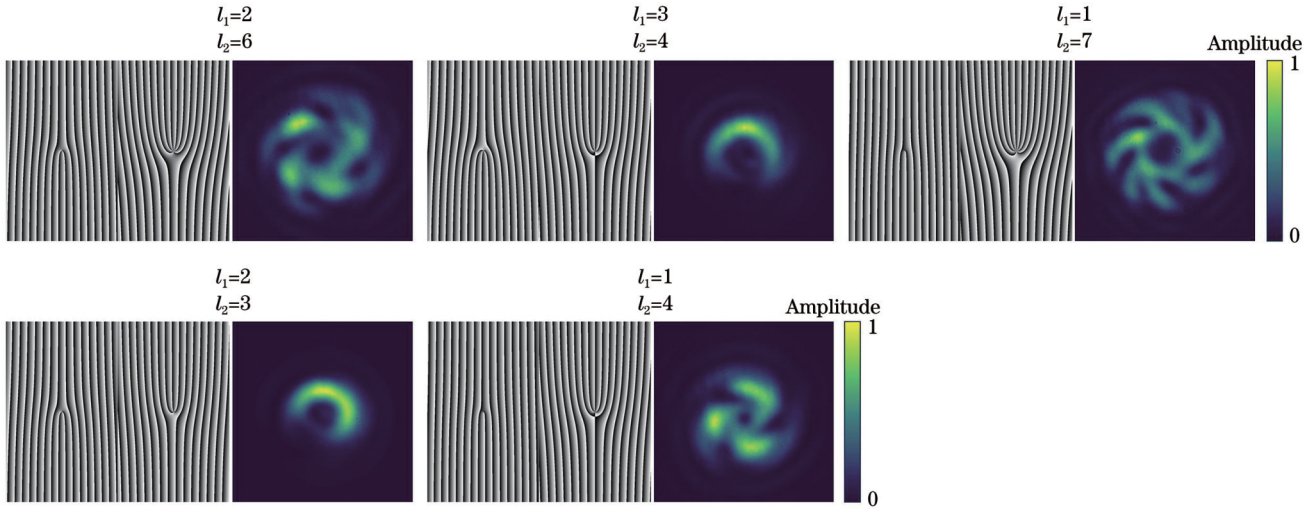


图9 拓扑荷数绝对值不等、符号为正的LG涡旋光束叠加态与对应的全息光栅图

Fig. 9 LG vortex beam superpositions with unequal absolute value of positive topological charges, and corresponding holographic gratings

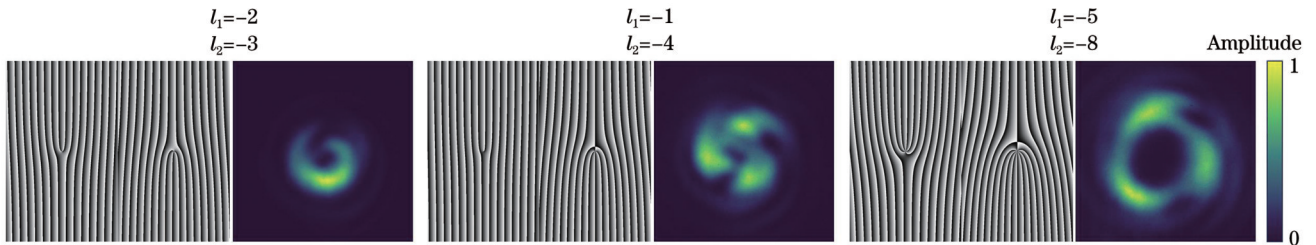


图10 拓扑荷数绝对值不等、符号为负的LG涡旋光束叠加态与对应的全息光栅图

Fig. 10 LG vortex beam superpositions with unequal absolute value of negative topological charges, and corresponding holographic gratings

需要注意的是,相比仿真结果,实验所得到的拓扑荷数不等的涡旋叠加光斑表现出旋转漂移形态。根据已有文献[53],这种现象是由光束离焦且存在涡旋相位所致。将图7与图8~10相对比,可观察到图7中的涡旋叠加花瓣没有发生变形,而图8~10中的涡旋叠加态则呈现出明显的旋转漂移形态,这是因为拓扑荷数绝对值相等、符号相反的涡旋叠加态的轨道角动量发生湮灭,而拓扑荷数绝对值不等的涡旋叠加态保留了螺旋相位结构,当光束在远离焦平面处会聚时,光场中各点的相位波前发生非均匀叠加,导致相位奇点扭曲、光强分布变形。通过观察图8~10中不同拓扑荷数的叠加光强可进一步发现,两个拓扑荷数相差越大,花瓣形态越扭曲,例如图8中 $l_1=-2$ 与 $l_2=3$ 的叠加花瓣与仿真结果较为相近,而 $l_1=-2$ 与 $l_2=6$ 的叠加花瓣变形较严重。此外,对比图9中 $l_1=1$ 与 $l_2=4$ 的叠加光强与图10中 $l_1=-1$ 与 $l_2=-4$ 的叠加光强可发现,前者呈现逆时针的旋转形态,而后者呈现顺时针的旋转形态,这是由两者的拓扑荷数不同所致:两个拓扑荷数相加为正则表现为逆时针旋转,相加为负则表现为顺时针旋转。同时,在对比中还观察到两种光束的光

强弥散程度不同,后者比前者的光强分布更为弥散,这是因为远离焦平面的程度不同,离焦平面越远,光强越弥散。

4 结 论

提出并展示了由随机光纤激光器产生的部分相干多奇点涡旋光束。对两个零阶LG光束的叠加态开展了仿真研究,结果表明拓扑荷数绝对值相等、符号相反的涡旋叠加态不具有螺旋相位分布,而拓扑荷数绝对值不等的涡旋叠加态因相位耦合会形成新的相位奇点。搭建了中心波长为1081.3 nm的随机分布式反馈光纤激光器,最高输出功率达2.26 W。以该随机光纤激光器为照明光源,通过搭建空间三角干涉光路实现涡旋光束的相干叠加,得到了具有丰富光强分布的多奇点涡旋光束,新生奇点围绕中心奇点呈均匀分布。总奇点数目为 $|l_1 - l_2| + 1$,且奇点数目可通过调节单个涡旋的拓扑荷数实现灵活调谐。这项工作有望拓展随机光纤激光器的应用范围,为粒子捕获、涡旋光复用通信和成像等领域提供光源。

参 考 文 献

- [1] Shen Y J, Wang X J, Xie Z W, et al. Optical vortices 30 years on: OAM manipulation from topological charge to multiple singularities[J]. *Light, Science & Applications*, 2019, 8: 90.
- [2] Forbes A, de Oliveira M, Dennis M R. Structured light[J]. *Nature Photonics*, 2021, 15: 253-262.
- [3] He C, Shen Y J, Forbes A. Towards higher-dimensional structured light[J]. *Light, Science & Applications*, 2022, 11: 205.
- [4] 刘俊, 王健. 涡旋光激光器研究进展[J]. *中国激光*, 2022, 49(12): 1201001.
Liu J, Wang J. Research progress of vortex laser[J]. *Chinese Journal of Lasers*, 2022, 49(12): 1201001.
- [5] 韦育, 于永河, 黑小兵, 等. 涡旋光束和光子计数在水下光通信中的应用[J]. *激光与光电子学进展*, 2022, 59(13): 1301001.
Wei Y, Yu Y H, Hei X B, et al. Application of vortex beam and photon counting in underwater optical communication[J]. *Laser & Optoelectronics Progress*, 2022, 59(13): 1301001.
- [6] Wan Z S, Wang H, Liu Q, et al. Ultra-degree-of-freedom structured light for ultracapacity information carriers[J]. *ACS Photonics*, 2023, 10(7): 2149-2164.
- [7] Huang S J, Miao Z, He C, et al. Composite vortex beams by coaxial superposition of Laguerre-Gaussian beams[J]. *Optics and Lasers in Engineering*, 2016, 78: 132-139.
- [8] Wan Z S, Shen Y J, Gong M L, et al. Quadrant-separable multi-singularity vortices manipulation by coherent superposed mode with spatial-energy mismatch[J]. *Optics Express*, 2018, 26(26): 34940-34955.
- [9] Zeng R Y, Yang Y J. Generation of an asymmetric optical vortex array with tunable singularity distribution[J]. *Journal of the Optical Society of America A*, 2021, 38(3): 313-320.
- [10] Gu L L, Cao Q, Zhan Q W. Spatiotemporal optical vortex wavepackets with phase singularities embedded in multiple domains[J]. *Chinese Optics Letters*, 2023, 21(8): 080003.
- [11] Anguita J A, Herreros J, Djordjevic I B. Coherent multimode OAM superpositions for multidimensional modulation[J]. *IEEE Photonics Journal*, 2014, 6(2): 7900811.
- [12] Qiao Z, Wan Z Y, Xie G Q, et al. Multi-vortex laser enabling spatial and temporal encoding[J]. *Photonix*, 2020, 1(1): 13.
- [13] Feng F, Hu J B, Guo Z F, et al. Deep learning-enabled orbital angular momentum-based information encryption transmission[J]. *ACS Photonics*, 2022, 9(3): 820-829.
- [14] Fu S Y, Shang Z J, Hai L, et al. Orbital angular momentum comb generation from azimuthal binary phases[J]. *Advanced Photonics Nexus*, 2022, 1(1): 016003.
- [15] 王明军, 余文辉, 黄朝军. 水下拉盖尔-高斯涡旋光束及其叠加态传输特性[J]. *光学学报*, 2023, 43(6): 0626001.
Wang M J, Yu W H, Huang C J. Transmission characteristics of underwater laguerre-gaussian vortex beam and its superposition states[J]. *Acta Optica Sinica*, 2023, 43(6): 0626001.
- [16] Li L, Guo Y C, Zhang Z C, et al. Photon total angular momentum manipulation[J]. *Advanced Photonics*, 2023, 5(5): 056002.
- [17] 樊鑫豪, 武炫光, 周亮, 等. 基于超表面的阵列光场纵向维度信息编解码[J]. *中国激光*, 2023, 50(18): 1813013.
Fan X H, Wu X G, Zhou L, et al. Longitudinally encoding and decoding information in light field arrays based on metasurface[J]. *Chinese Journal of Lasers*, 2023, 50(18): 1813013.
- [18] Tian Y H, Wang L L, Duan G Y, et al. Multi-trap optical tweezers based on composite vortex beams[J]. *Optics Communications*, 2021, 485: 126712.
- [19] Hong L, Guo H X, Qiu X D, et al. Experimental optical computing of complex vector convolution with twisted light[J]. *Advanced Photonics Nexus*, 2023, 2(4): 046008.
- [20] Chen Y H, Wang F, Cai Y J. Partially coherent light beam shaping via complex spatial coherence structure engineering[J]. *Advances in Physics X*, 2022, 7(1): 2009742.
- [21] Yu J Y, Huang Y, Wang F, et al. Scintillation properties of a partially coherent vector beam with vortex phase in turbulent atmosphere[J]. *Optics Express*, 2019, 27(19): 26676-26688.
- [22] 杨茜, 周泽中, 刘恺, 等. 频率间隔可切换多波长布里渊随机光纤激光器[J]. *中国激光*, 2022, 49(11): 1101003.
Yang Q, Zhou Z Z, Liu K, et al. Frequency interval switchable multi-wavelength Brillouin random fiber laser[J]. *Chinese Journal of Lasers*, 2022, 49(11): 1101003.
- [23] 齐逸飞, 林圣淘, 包兴宇, 等. 基于光谱快速探测的光纤随机激光动态传感[J]. *激光与光电子学进展*, 2023, 60(11): 1106027.
Qi Y F, Lin S T, Bao X Y, et al. Random fiber laser dynamic sensing based on rapid spectral detection[J]. *Laser & Optoelectronics Progress*, 2023, 60(11): 1106027.
- [24] Gomes A S L, Moura A L, de Araújo C B, et al. Recent advances and applications of random lasers and random fiber lasers[J]. *Progress in Quantum Electronics*, 2021, 78: 100343.
- [25] Han B, Wu H, Liu Y, et al. Ultralong single-ended random fiber laser and sensor[J]. *Laser & Photonics Reviews*, 2023, 17(6): 2200797.
- [26] Ye J, Zhang Y, Liang J R, et al. 2 kW random fiber laser based on hybrid Yb-Raman gain[J]. *Chinese Optics Letters*, 2023, 21(9): 090004.
- [27] Churkin D V, Sugavanam S, Vatik I D, et al. Recent advances in fundamentals and applications of random fiber lasers[J]. *Advances in Optics and Photonics*, 2015, 7(3): 516-569.
- [28] Turitsyn S K, Babin S A, El-Taher A E, et al. Random distributed feedback fibre laser[J]. *Nature Photonics*, 2010, 4(4): 231-235.
- [29] Li Y X, Deng J C, Shen M, et al. Modeless Raman fiber laser[J]. *Optica*, 2023, 10(8): 1037-1043.
- [30] 范孟秋, 林圣淘, 吴函, 等. 随机分布反馈光纤激光器时-频-空域特性研究进展[J]. *强激光与粒子束*, 2021, 33(11): 111003.
Fan M Q, Lin S T, Wu H, et al. Research progress of random fiber lasers' characteristics in time-frequency-spatial domain[J]. *High Power Laser and Particle Beams*, 2021, 33(11): 111003.
- [31] Ma R, Li J Q, Guo J Y, et al. High-power low spatial coherence random fiber laser[J]. *Optics Express*, 2019, 27(6): 8738-8744.
- [32] Wang S S, Zhang W L, Yang N, et al. High-power multimode random fiber laser for speckle-free imaging[J]. *Annalen der Physik*, 2021, 533(12): 2100390.
- [33] Ma R, Rao Y J, Zhang W L, et al. Multimode random fiber laser for speckle-free imaging[J]. *IEEE Journal of Selected Topics in Quantum Electronics*, 2019, 25(1): 0900106.
- [34] Ma R, Wang Z, Zhang H H, et al. Imaging through opacity using a near-infrared low-spatial-coherence fiber light source[J]. *Optics Letters*, 2020, 45(13): 3816-3819.
- [35] Guo J Y, Zhang W L, Rao Y J, et al. High contrast dental imaging using a random fiber laser in backscattering configuration[J]. *OSA Continuum*, 2020, 3(4): 759-766.
- [36] Guo J Y, Rao Y J, Zhang W L, et al. Dental imaging with near-infrared transillumination using random fiber laser[J]. *Photonic Sensors*, 2020, 10(4): 333-339.
- [37] Wu H, Han B, Wang Z N, et al. Temporal ghost imaging with random fiber lasers[J]. *Optics Express*, 2020, 28(7): 9957-9964.
- [38] Wang L L, Qi T C, Liu Z T, et al. Complex pattern transmission through multimode fiber under diverse light sources[J]. *APL Photonics*, 2022, 7(10): 106104.
- [39] Du X Y, Zhang H W, Ma P F, et al. Spatial mode switchable fiber laser based on FM-FBG and random distributed feedback[J]. *Laser Physics*, 2015, 25(9): 095102.
- [40] Ma X Y, Ye J, Zhang Y, et al. Vortex random fiber laser with controllable orbital angular momentum mode[J]. *Photonics*

- Research, 2021, 9(2): 266-271.
- [41] Zulkifli M Z, Lau K Y, Muhammad F D, et al. Dual-mode output in half open cavity random fibre laser[J]. Optics Communications, 2019, 430: 273-277.
- [42] Wang J H, Chen R S, Yao J N, et al. Random distributed feedback fiber laser generating cylindrical vector beams[J]. Physical Review Applied, 2019, 11(4): 044051.
- [43] Lü J L, Li H X, Zhang Y M, et al. Few-mode random fiber laser with a switchable oscillating spatial mode[J]. Optics Express, 2020, 28(26): 38973-38982.
- [44] Lü J L, Li H X, Zhang Y M, et al. Tailoring the spectrum and spatial mode of Yb-doped random fiber laser[J]. Optics Express, 2022, 30(5): 8345-8355.
- [45] Xu J T, Wang L T, Zhang L K, et al. Dynamic mode-switchable and wavelength-tunable Brillouin random fiber laser by a high-order mode pump[J]. Optics Express, 2021, 29(21): 34109-34117.
- [46] Luo K H, Ma R, Wu H, et al. Flexible generation of broadly wavelength- and OAM-tunable Laguerre-Gaussian (LG) modes from a random fiber laser[J]. Optics Express, 2023, 31(19): 30639-30649.
- [47] Yu G Y, Huang Z, Ma R, et al. High power vortex random lasing in an all-fiber structure[J]. Optics & Laser Technology, 2023, 162: 109283.
- [48] 于观玉, 张春香, 黄政, 等. 基于光纤随机激光的 1.7 μm 波段高功率涡旋光束产生[J]. 光学学报, 2023, 43(22): 2214003. Yu G Y, Zhang C X, Huang Z, et al. 1.7 μm high-power vortex beam generation based on random fiber lasers[J]. Acta Optica Sinica, 2023, 43(22): 2214003.
- [49] Fu S Y, Gao C Q. Optical vortex beams: fundamentals and techniques[M]. Singapore: Springer Nature Singapore, 2023.
- [50] Agrawal G P. Nonlinear fiber optics[M]. 6th ed. Cambridge: Academic Press, 2019.
- [51] Ye J, Ma X Y, Zhang Y, et al. Revealing the dynamics of intensity fluctuation transfer in a random Raman fiber laser[J]. Photonics Research, 2022, 10(3): 618-627.
- [52] Wang Z, Bovik A C, Sheikh H R, et al. Image quality assessment: from error visibility to structural similarity[J]. IEEE Transactions on Image Processing, 2004, 13(4): 600-612.
- [53] Dai X B, Li Y Q, Liu L H, et al. The defocused helical structure of two superposed vortex beams[J]. Proceedings of SPIE, 2018, 10847: 108470Z.

Multi-Singularity Vortex Beam Generated by Random Fiber Laser

Ma Xiaoya¹, Ye Jun^{1,2,3}, Liang Junrui¹, He Junhong¹, Zhang Yang¹, Xu Jiangming^{1*},
Zhou Pu^{1**}, Jiang Zongfu^{1,2,3}

¹College of Advanced Interdisciplinary Studies, National University of Defense Technology, Changsha 410073, Hunan, China;

²Nanhu Laser Laboratory, National University of Defense Technology, Changsha 410073, Hunan, China;

³Hunan Provincial Key Laboratory of High Energy Laser Technology, National University of Defense Technology, Changsha 410073, Hunan, China

Abstract

Objective In the context of multifunctional operation and diversified application requirements, how to expand the controllable degrees of freedom of vortex beams has become an urgent scientific problem to be solved. Compared to traditional vortex beams with one phase singularity, multi-singularity vortex beams generated by vortex coherent superposition can achieve precise control on phase singularities, significantly enriching the control methods of phases in structured light fields. Light sources are crucial for the application of structured beams. Compared to highly coherent structured beams, partially coherent structured beams are proven to have the ability of anti-turbulence scintillation and speckle suppression, which demonstrate significant advantages in atmospheric transmission and imaging. As a common partially coherent fiber laser, random fiber lasers (RFLs) which employ Rayleigh scattering in passive fibers to provide random distributed feedback are widely adopted as illumination sources for structured light fields. Currently, various typical structured beams such as LP₁₁ mode, vortex beam, and cylindrical vector beam have been generated and controlled based on RFLs. However, there are no reports on RFL-based multi-singularity vortex beams. The combination of the partial coherence of RFLs and singularity control of structured beams can expand the multidimensional manipulation of structured light fields, and the application scope in many fields such as optical tweezers, free-space communication, and speckle correlation imaging. Here, multi-singularity vortex beams generated by an RFL are firstly proposed and demonstrated. The RFL with a central wavelength of 1081.3 nm is constructed and employed as the illumination. By coherent superposition between Laguerre-Gaussian (LG) beams with different topological charges, multi-singularity vortex beams with controllable singularity numbers are achieved.

Methods Coherent superposition of two zero-order LG beams is simulated and analyzed. The distribution of superimposed light field is given by Eq. (4), and intensity and phase distributions of superposition states with different

topological charges are obtained. The RFL is experimentally built with a backward-pumped half-opened cavity, as shown in Fig. 5(a). The pump light is provided by a 1030 nm ytterbium-doped fiber oscillator, and the output end is connected with a cladding power stripper (CPS) to filter out the cladding light. A circulator (Cir) is mounted after the CPS to protect the pump source from backward light. Subsequently, by employing a 1030 nm/1080 nm wavelength division multiplexer (WDM), the 1030 nm pump light is injected into a 5 km single-mode fiber (SMF) with a core/cladding diameter of 8 μm /125 μm . The generated 1081.3 nm signal light is reflected by a highly reflective fiber Bragg grating (HR FBG, the center wavelength of 1081.3 nm and reflective bandwidth of 0.07 nm), and then it is emitted via the WDM. The laser gain of the RFL is provided by stimulated Raman scattering in the SMF, and the feedback is offered by both random distributed scattering in the SMF and point feedback of the HR FBG. By utilizing the RFL as the illumination, a spatially optical path is constructed to generate a multi-singularity structured light field [Fig. 5(b)]. The Gaussian beam from the RFL is firstly collimated and expanded, and then transmitted into horizontally polarized beam with high polarization degree and adjustable intensity by two polarization beam splitters (PBS1, PBS2) and a half wave plate (HWP). After a 50:50 non-polarization beam splitter (BS), the horizontally polarized beam is divided into a transmitted beam and a reflected beam, which are incident at different positions of the spatial light modulator (SLM) after being reflected. By loading different phase maps on the SLM, two vortex beams with different topological charges can be obtained. Meanwhile, interference is conducted on the two vortex beams by the BS to form a vortex superposition state with multiple singularities. The intensity of the superimposed beam is focused via a lens and collected by a CCD camera.

Results and Discussions The superimposed intensity distributions of zero-order LG beams with different topological charges perform petal patterns, and the number of petals is $|l_1 - l_2|$. Meanwhile, the phase distributions of the superimposed beams vary according to different topological charges. The phase distributions obtained by superimposing two zero-order LG beams with equal absolute value and opposite signs of topological charges are shown in Fig. 1, with no spiral phase wavefront. Superposition states generated by zero-order LG beams with unequal absolute values of topological charges are described in Figs. 2, 3, and 4, and have the characteristic of spiral phase wavefront with newborn phase singularities due to phase coupling. The newborn singularity number is $|l_1 - l_2|$, and the total singularity number is $|l_1 - l_2| + 1$. The topological charge of the central singularity corresponds to the topological charge of the LG beam with a smaller diameter. The absolute values of topological charges of the newborn singularities are 1, which are uniformly distributed around the central singularity.

The output characteristics of the RFL are demonstrated in Fig. 6. The central wavelength of the random laser is located at 1081.3 nm with a generation threshold of 2.36 W and a maximum power of 2.26 W, corresponding to a slope efficiency of 58.91%. Further power enhancement is limited by the stimulated Raman scattering effect. The 3 dB bandwidth of the RFL gradually widens with the increasing pump power, reaching a maximum of 0.23 nm. The vortex superposition states using the RFL as the illumination are plotted in Figs. 7 and 8. The experimental beam spots are consistent with the simulation results. By changing the topological charge of the LG beam, the singularity number of the generated multi-singularity vortex beam can be flexibly switched.

Conclusions Partially coherent multi-singularity vortex beams generated by an RFL are firstly proposed and demonstrated. The superposition state of two zero-order LG beams is simulated. The results indicate that vortex superposition states with equally absolute values and opposite signs of topological charges show no spiral phase distribution, while the states with unequal absolute values of topological charges generate new phase singularities due to phase coupling between the two LG beams. Additionally, a random distributed feedback fiber laser with a central wavelength of 1081.3 nm is constructed, with a maximum output power of 2.26 W. By employing the RFL as the illumination, a spatially triangular interference path is built to achieve coherent superposition of vortex beams. Multi-singularity vortex beams with various intensity distributions are generated, and newborn singularities are uniformly distributed around the central singularity. The total singularity number is $|l_1 - l_2| + 1$, which can be flexibly tuned by adjusting the topological charges of the two LG beams. This work may expand the application scope of RFLs, and provide light sources for many fields such as particle trapping, vortex optical multiplexing communication, and imaging.

Key words lasers; random fiber laser; multi-singularity vortex beam; vortex superposition; singularity controllability; partial coherence